Green Chemistry

PAPER

Insights into the stability of gold nanoparticles supported on metal oxides for the base-free oxidation of glucose to gluconic acid†

Cite this: *Green Chem.*, 2014, **16**, 719

Yuran Wang, Stijn Van de Vyver, Krishna K. Sharma and Yuriy Román-Leshkov*

Received 10th July 2013,
Accepted 12th August 2013

DOI: 10.1039/c3gc41362d

www.rsc.org/greenchem

Gold (Au) catalysts have been rarely investigated for the oxidation of glucose in the absence of a base. These conditions are critical, however, to enable the sequential one-pot combination of cellulose hydrolysis and glucose oxidation. Here we evaluate the catalytic performance and stability of Au nanoparticles supported on metal oxides for the oxidation of glucose to gluconic acid under unadjusted pH and acidic conditions. The study provides insights into the deactivation of the catalysts caused by leaching and hydrothermal sintering of Au nanoparticles, as well as by adsorption of reactive species. We found that lowering the surface density of Au on metal oxides decreases the sintering rate of the Au nanoparticles and hence enhances the stability and activity of the catalysts.

1. Introduction

Aldonic and aldaric acids have emerged as highly attractive chemical intermediates that can be used in a variety of applications.[1–3] One such compound, D-gluconic acid (100 000 tons per year), is widely used in the food, pharmaceutical, paper and concrete industries.[4–6] Gluconic acid and its salts are currently produced by the enzymatic oxidation of D-glucose by *Aspergillus niger* and *Gluconobacter suboxydans*.[1] One of the impediments to the large-scale application of the fermentation processes is that they necessitate the neutralisation of the acid in order to avoid deactivation of the enzymes.[7] This means that there is a need to develop heterogeneous catalysts that can catalyze the oxidation of D-glucose under base-free conditions.

The benefits of using gold (Au) catalysts for the aerobic oxidation of carbohydrates have been well researched and documented in recent years.[2,8] Key features include exceptionally high catalytic activities and selectivities for the oxidation of pentoses[9,10] and hexoses[4,6,10–21] even at relatively low temperatures (40–65 °C). Also, it has been shown that Au can catalyze the oxidation of glucose without pH control, thus allowing the production of gluconic acid, not its salt, under slightly acidic conditions.[12] It has been demonstrated that such conditions can enable the one-pot combination of acid-catalyzed hydrolysis reactions with Au-catalyzed glucose oxidation.[22–24] This kind of catalytic cascade reaction is primarily important for the depolymerization and valorization of cellulose,[7,25–27] although it might also be relevant to the catalytic processing of other di-, oligo-, and polysaccharides.

Most studies on the stability of Au catalysts so far have concerned the oxidation of glucose in the presence of a base. Initially, Biella *et al.* studied the recycling of Au on activated carbon (Au/AC) at pH values from 7.0 to 9.5.[12] They found a decrease in activity of more than 50% after four consecutive runs, mainly due to leaching and sintering of the Au particles. In contrast, Au on metal oxide catalysts are typically more stable under basic conditions. For example, Au/Al_2O_3 and Au/TiO_2 catalysts could be successfully reused for the oxidation of glucose and disaccharides at pH 9.[6,10,28,29] Thielecke *et al.* even demonstrated the long-term stability of Au/Al_2O_3 in a continuous-flow system.[4,13] However, comparatively little is known about the stability of such catalysts under acidic conditions.

In this contribution, we report on the use of Au supported on nano- or microsized metal oxides. Au on nanosized ceria ($Au/nCeO_2$), for example, has recently been shown to be a relatively stable catalyst for the oxidative esterification of 5-hydroxymethyl-2-furfural into 2,5-dimethylfuroate under base-free conditions.[30] The choice of support influences both the dispersion and the electronic state of Au nanoparticles (Au NPs),[31] leading us to investigate a series of metal oxides including ceria, titania and zirconia. The immobilization of Au NPs on such supports can be achieved by the deposition–precipitation method.[32] Avoiding agglomeration and

Department of Chemical Engineering, Massachusetts Institute of Technology, 77 Massachusetts Avenue, Cambridge, MA 02139, USA. E-mail: yroman@mit.edu; Tel: +617-253-7090

† Electronic supplementary information (ESI) available: Additional experimental information, N_2 adsorption/desorption isotherms of μCeO_2 and $nCeO_2$, TGA curve of the spent 0.02 wt% $Au/\mu CeO_2$ catalyst, Au particle size distribution histograms of the catalysts discussed in the Section 3.5 of the manuscript. See DOI: 10.1039/c3gc41362d

sintering of the Au NPs during thermal activation is a great challenge since the catalytic activity markedly decreases for Au particles larger than 10 nm.[33] It is argued that Au species are comparatively more stable when formed by the deposition–precipitation method than when they are prepared by *e.g.* anionic adsorption, leading to significantly smaller, and hence more active, Au NPs.[32] Another factor that determines the size of Au particles is the metal–support interaction.[11] It is understandable that a higher Fermi level of the support material can lead to a stronger electronic interaction with the Au NPs and in turn a reduced tendency for agglomeration.[31]

The aim of this study was to evaluate the catalytic performance and stability of Au NPs supported on various metal oxides for the base-free oxidation of glucose to gluconic acid. The key aspect that distinguishes our approach from most of the previous studies is that the pH of the reaction solution was either unadjusted or lowered by the addition of H_2SO_4.

2. Experimental section

2.1. Preparation of Au catalysts

Nanosized ceria and zirconia, hereafter referred to as $nCeO_2$ and $nZrO_2$, were synthesized according to a previously reported method.[30] Briefly, an aqueous solution of $Ce(NO_3)_3{\cdot}6H_2O$ or $ZrO(NO_3)_2{\cdot}xH_2O$ (0.8 M, 375 mL) was added to a solution of NH_4OH in deionized water (0.8 M, 1.1 L). After stirring for 30 min, the solution was aged at 100 °C for 24 h in a polyethylene vessel. The mixture was cooled down, filtered and washed with an excess amount of deionized water. The resulting particles were dried under vacuum and calcined under an air flow of 100 mL min^{-1} at 400 °C for 4 h. The other support materials were purchased from Sigma Aldrich and used as received (see ESI†).

Au was deposited on the metal oxides by the deposition–precipitation method.[30] A solution of $HAuCl_4{\cdot}3H_2O$ (175 mg) in deionized water (80 mL) was brought to pH 10 by adding a NaOH solution (0.2 M). This solution was mixed with a suspension containing the metal oxide (2 g) in deionized water (25 mL). After stirring for 18 h, the suspension was filtered and washed with an excess amount of deionized water until no more chlorine could be detected by the AgCl test. The supported Au catalyst was dried overnight at 80 °C and then reduced for 4 h at 225 °C in 5% H_2 in N_2 (100 mL min^{-1}).

The Au/AC catalyst was prepared according to the procedure reported by Biella *et al.*[12] A solution of $HAuCl_4{\cdot}3H_2O$ (1 L, 100 μg mL^{-1}) was mixed with 2.5 g of a 2 wt% solution of poly (vinyl alcohol) (PVA, $M_W \sim 10\,000$). To this solution, 0.1 M $NaBH_4$ solution (20 mL) was added dropwise, leading to the formation of metallic Au NPs. The PVA stabilized Au NPs were then immobilized on activated carbon (Darco®, 100 mesh) by adding 2 g of the support. The as-synthesized Au/AC catalyst was filtered after 2 h and washed with deionized water.

2.2. Characterization of the catalysts

Transmission electron microscopy (TEM) measurements were performed using either a JEOL TEM-200CX microscope operated at 120 kV or a JEOL TEM 2011 microscope operated at 200 kV. Samples were deposited on the TEM grids after ultrasonic dispersion in ethanol. The Au loading of the metal oxide catalysts was determined by inductively coupled plasma atomic emission spectrometry (ICP-AES) using an ICP analyzer (HORIBA JOBIN YVON). The Au loading of the Au/AC catalyst was analyzed by X-ray fluorescence using a Bruker Tracer III-SD Handheld X-Ray Fluorescence spectrometer. Nitrogen adsorption–desorption isotherms were recorded using a Quantachrome Autosorb iQ at liquid nitrogen temperature (−196 °C). Prior to the physisorption measurements, the samples were degassed for 2 h under vacuum at 400 °C. X-ray photoelectron spectroscopy (XPS) was performed using a PHI Versaprobe II equipped with a monochromatic aluminium anode X-ray source and a dual-beam charge neutralization system with an electron neutralizer bias of 1.2 eV and an Ar ion beam energy of 10 eV. The C1s peak was used as a reference and shifted to 284.8 eV for charge correction. Themogravimetric analysis (TGA) was performed by heating the catalyst under a flow of 10 mL min^{-1} N_2 and 90 mL min^{-1} air, using a Q500 thermal analysis system (TA Instruments). About 30–50 mg of the sample was heated at 2 °C min^{-1} up to 600 °C.

The dispersion of Au NPs was calculated as the ratio of the number of external Au atoms ($N_{\text{surface Au}}$) to the total number of Au atoms ($N_{\text{total Au}}$). The values of $N_{\text{surface Au}}$ and $N_{\text{total Au}}$ were estimated based on the assumption that the Au NPs can be modelled as an fcc crystal lattice:[34]

$$N_{\text{surface Au}} = 10m^2 - 20m^2 + 12 \quad (1)$$

$$N_{\text{total Au}} = \frac{(10m^3 - 15m^2 + 11m - 3)}{3} \quad (2)$$

$$D_m = 1.105 \times D_{\text{atom}} \times \sqrt[3]{N_{\text{total Au}}} \quad (3)$$

with m equal to the number of shells, D_m equal to the TEM-determined mean diameter of the Au NPs, and D_{atom} equal to the atomic diameter of Au (0.288 nm).

2.3. Oxidation reactions and product analysis

The catalytic reactions were carried out with solutions of glucose in deionized water (167 mmol L^{-1}) at an initial pH of 4. In some experiments the initial pH was adjusted to 1.6 by the addition of small amounts of H_2SO_4. The reaction mixture was pressurized with O_2 to 2.3 bar and stirred at 65 °C in a pressure reaction vessel (Andrews Glass Co.). The catalysts were recovered at the end of each run by centrifugation and washed with deionized water for at least 5 times until the supernatant reached the pH of deionized water. An alkaline wash was done with a 0.1 M NaOH solution. In both cases, the washed catalysts were dried at 80 °C prior to reuse. Regeneration of the $Au/\mu CeO_2$ catalyst was performed by calcination for 4 h at the temperatures specified in Section 3.5 with a flow rate of 10 mL min^{-1} N_2 and 90 mL min^{-1} air.

Liquid samples were syringe filtered (0.2 μm PTFE membrane) and analyzed using an Agilent 1260 HPLC. The

carbohydrates were separated on a Bio-Rad Aminex HPX-87C column at 80 °C and detected with an evaporative light scattering detector, using deionized water as the mobile phase at a flow rate of 0.6 mL min^{-1}. In parallel, organic acids were separated on a Bio-Rad Aminex HPX-87H column at 30 °C and detected with a UV-Vis detector at 210 nm, using 8 mM H_2SO_4 in deionized water as the mobile phase at a flow rate of 0.6 mL min^{-1}. Dried aliquots of the samples were trimethylsilylated according to a previously reported protocol[35,36] and analyzed by GC–MS. The conversion of glucose and the selectivity to gluconic acid were calculated on a molar basis.

3. Results and discussion

3.1. Catalyst screening

A series of Au supported on metal oxides was prepared, characterized and tested for the base-free oxidation of glucose to gluconic acid. Table 1 shows the Au loading, the mean particle size and the dispersion of the Au NPs, as well as typical catalytic results. Prefixes n and μ refer to nano- and microsized metal oxide supports with particle sizes smaller than 30 nm and larger than 100 nm, respectively. All of the Au NPs supported on metal oxides were highly active for glucose oxidation under base-free conditions, with conversions of glucose ranging between 24% and 91% after 2 h of reaction. For comparison, a benchmark Au/AC catalyst with 0.6 wt% Au loading showed only 7% conversion.

As for the selectivity to gluconic acid, the values in Table 1 agree well with previously reported data for Au-based catalysts under acidic conditions.[12] A GC–MS analysis after trimethylsilylation of the product mixture showed the presence of glycolic acid, C_5 aldonic acids and the δ-lactone of gluconic acid as the most important byproducts of this reaction.

Ishida *et al.* previously reported that the size of Au particles, and hence their catalytic activity, depend strongly on the preparation method.[11] The deposition–precipitation method used in this study gave Au NPs with mean particle sizes ranging from 1.7 nm to 3.0 nm (fourth column in Table 1). The most promising results overall were obtained for TiO_2 and CeO_2—the latter being known for its capability to store oxygen and to become reduced.[37–40] There is, however, no correlation in Table 1 between the size of the Au NPs and the catalytic activity.

The formation of gluconic acid induced a significant pH decrease of the reaction solution. For the experiments under unadjusted pH, typical pH values measured at room temperature ranged from 4.0 to 2.5 before and after the reaction, respectively. To evaluate the performance of the catalysts under acidic conditions, parallel experiments were performed at an initial pH of 1.6 by the addition of small amounts of H_2SO_4 (the last two columns in Table 1). Lowering the pH caused a decrease of the reaction rate, which is in agreement with the study by Biella *et al.*[12] The inhibiting effect of the acidic conditions is reflected in lower glucose conversions; however, the impact on the catalytic activity is relatively small for Au on nanosized metal oxides. The selectivity to gluconic acid remained ≥88% regardless of the pH conditions used. Entries 1–2 and 5–6 in Table 1 show the effect of Au loading on the catalytic activity of Au/nCeO_2 and Au/μCeO_2. When decreasing the Au loading of these catalysts, the conversion of glucose remained approximately constant for Au/nCeO_2; however, for Au/μCeO_2 under acidic conditions, the conversion increased from 37% to 59% upon decreasing the loading from 1.1% to 0.6%. Hence, lowering the Au loading seems to increase the activity of Au/μCeO_2 under acidic conditions. This result prompted us to study the stability of both catalysts under the given conditions.

3.2. Comparison of the stability of Au/μCeO_2 and Au/nCeO_2

Recycling and reuse experiments provided further information on the stability of the Au catalysts. Fig. 1 compares the evolution of the activity of 0.6 wt% Au/μCeO_2 and 0.5 wt% Au/nCeO_2 over consecutive reaction cycles. The catalysts were filtered, washed with deionized water and dried after each run.

The experiments of Fig. 1(a) were carried out without pH adjustment of the reaction solution. It can be seen that by the fourth cycle, the conversion of glucose over Au/μCeO_2 decreased from 87% to 33%. Au/nCeO_2 was less prone to deactivation, as in this case the conversion decreased from 87%

Table 1 Base-free catalytic oxidation of glucose with Au NPs supported on different metal oxides[a]

					Unadjusted pH		Initial pH of 1.6	
Entry	Catalyst support	Au loading[b] (wt%)	D^c (nm)	Dispersion[d]	Conv. (%)	Select. (%)	Conv. (%)	Select. (%)
1	nCeO_2	0.5	1.8	0.60	74	95	67	96
2	nCeO_2	1.4	2.5	0.47	75	99	75	96
3	nZrO_2	1.6	1.7	0.62	89	99	86	97
4	nTiO_2	1.3	3.0	0.40	91	99	81	98
5	μCeO_2	0.6	2.0	0.55	76	96	59	90
6	μCeO_2	1.1	2.9	0.41	77	98	37	90
7	μZrO_2	0.8	2.1	0.53	65	98	24	88
8	μTiO_2	1.2	2.0	0.55	89	98	54	>99

[a] Reaction conditions: glucose 167 mmol L^{-1}, 12 mL, pO_2 = 2.3 bar, 65 °C, glucose/Au = 140, unadjusted pH, 2 h. [b] Au loading determined by ICP-AES. [c] Mean Au particle diameter determined by TEM analysis and based on a count of at least 100 Au NPs. [d] Dispersion of the Au NPs calculated assuming a predominantly cuboctahedral structure of the Au NPs (see the Experimental section).

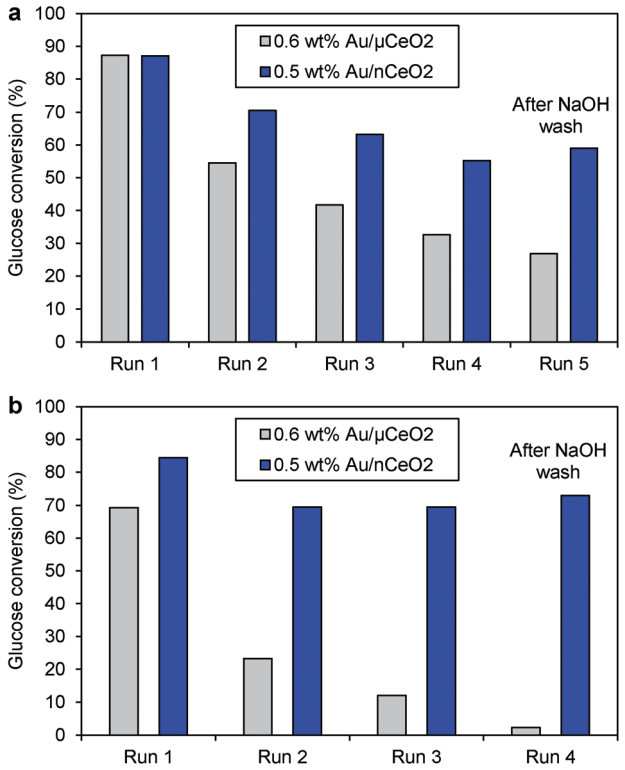

Fig. 1 Conversion of glucose over Au/μCeO_2 and Au/$nCeO_2$ measured after 4 h of reaction (a) under unadjusted pH and (b) at an initial pH of 1.6. The catalysts were washed with an NaOH solution before the last reaction cycle. Reaction conditions: glucose 167 mmol L^{-1}, 12 mL, pO_2 = 2.3 bar, 65 °C, glucose/Au = 140.

to 55%. Our initial strategy to recover the catalytic activity was based on a study by Abad *et al.*,[34] who showed that a NaOH wash can remove strongly adsorbed carboxylic acid species. This method was applied to the catalysts recovered after the fourth reaction cycle. In our case, however, the NaOH wash did not result in significant changes of the catalytic activity. Instead, we suspected that one of the major causes of the deactivation of Au/μCeO_2 was Au leaching. ICP-AES analysis showed that this catalyst had lost about 55% of its original Au loading during the oxidation reaction. Notably, the Au/$nCeO_2$ catalyst had lost less than 2% of its Au loading after five cycles.

Consistent with the approach in Table 1, we also investigated the effect of lowering the pH of the reaction solution. Fig. 1(b) shows that the catalytic activity of 0.6 wt% Au/μCeO_2 decreased drastically under acidic conditions compared to that under the unadjusted pH conditions. Specifically, the conversion of glucose over 0.6 wt% Au/μCeO_2 decreased from 69% (run 1) to 12% (run 3) on adding H_2SO_4 to the reaction solution. In contrast, only a slight decrease in catalytic activity was observed for 0.5 wt% Au/$nCeO_2$. ICP-AES analysis showed no significant Au leaching for Au/$nCeO_2$, while Au/μCeO_2 lost 74% of its Au loading after four reaction cycles. As such, the distinct stability properties of the two catalysts required additional studies.

3.3. Effect of the Au particle surface density on the catalyst stability

Au leaching cannot fully account for the observed decrease in activity, and hence we investigated the sensitivity of the Au NPs to sintering in order to gain further insight into the deactivation mechanisms. Fig. 2 shows TEM images of the 0.6 wt% Au/μCeO_2 and 0.5 wt% Au/$nCeO_2$ catalysts prior to and after reaction, while Fig. 3 displays the evolution of the Au particle size distribution during several reaction cycles. The TEM-based investigation reveals that the textural properties of the metal oxide support, such as its size and surface area, are key factors in determining the size and stability of the Au NPs.[41]

The histograms in Fig. 3 indicate relatively narrow Au particle size distributions of the as-synthesized catalysts, irrespective of whether μCeO_2 or $nCeO_2$ is used as the support. However, there is a vast difference in the evolution of the particle size distributions between the reused 0.6 wt% Au/μCeO_2 and 0.5 wt% Au/$nCeO_2$ samples. The former is notably more sensitive to sintering, which is consistent with the fact that this catalyst showed higher deactivation rates (Fig. 1). Acidic conditions accelerate Au sintering for both Au/$nCeO_2$ and Au/μCeO_2; however, the shift towards larger Au NP sizes is more pronounced for Au/μCeO_2 than for Au/$nCeO_2$. Indeed, the mean Au particle size for Au/μCeO_2 increased from 2.0 nm to 7.1 nm after the last reaction cycle (Fig. 3c), whereas the mean particle size for Au/$nCeO_2$ increased only from 1.3 nm to 1.9 nm (Fig. 3d). We hypothesized that the relatively stable nature of Au/$nCeO_2$ is due to the low surface density of the Au NPs. N_2 physisorption showed that the Brunauer–Emmett–Teller (BET) surface area of $nCeO_2$ (100 m^2 g^{-1}) is 25 times larger than the surface area of μCeO_2 (4 m^2 g^{-1}) (Fig. S1 in the

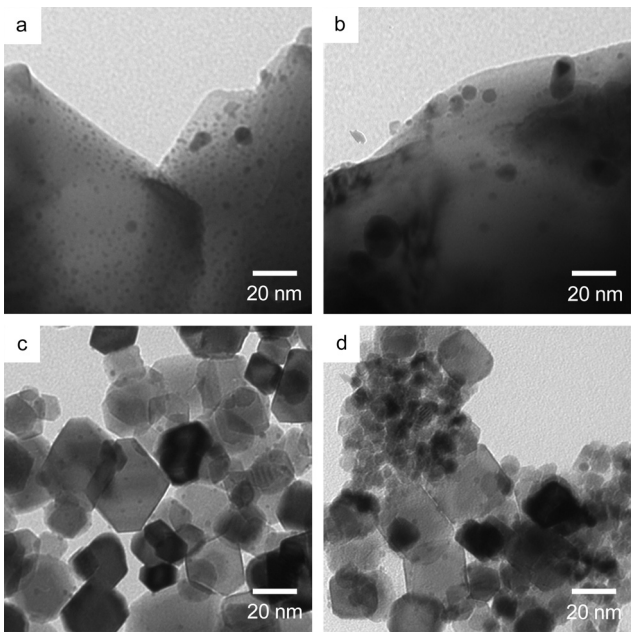

Fig. 2 Representative TEM images of the 0.6 wt% Au/μCeO_2 (a, b) and 0.5 wt% Au/$nCeO_2$ catalysts (c, d), before (left) and after use in glucose oxidation (right).

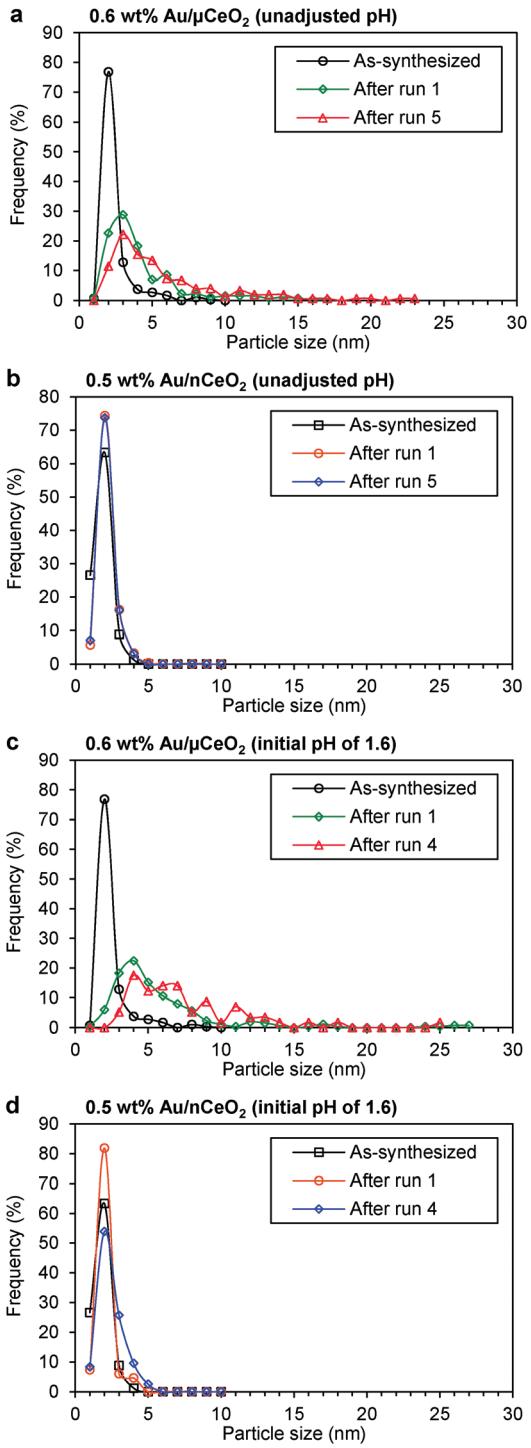

Fig. 3 Au particle size distribution histograms of 0.6 wt% Au/μCeO_2 (a, c) and 0.5 wt% Au/$nCeO_2$ (b, d). Reaction conditions: see Fig. 1.

ESI†). Since both catalysts have a similar Au loading, the surface density of the Au NPs is about 25 times higher for Au/μCeO_2 than for Au/$nCeO_2$. This seems to suggest that the interparticle distance determines the coalescence rate of the Au NPs and hence their tendency to sinter by the particle migration mechanism.[41–43] An alternative mechanism that sustains our experimental observations is based on a solution-mediated Ostwald ripening *via* Au dissolution and redeposition. Ostwald ripening could explain the observed correlation between the growth of the Au NPs and the extent of Au leaching of Au/μCeO_2 and Au/$nCeO_2$. The Au NPs are more susceptible to sintering during reactions at a lower pH, which, again, is in line with the general expectations given that the solubility of Au is higher under more acidic conditions.

The size of the CeO_2 support has important implications on the stability of the Au NPs. Given its higher density of defect sites (*i.e.*, mainly oxygen vacancies), $nCeO_2$ is known to have more anchoring sites than μCeO_2.[30] One prevalent view is that these anchoring sites can further stabilize the Au NPs against particle growth.[32,40,44] In this study, a higher number of defect sites on the surface of $nCeO_2$ probably helps to stabilize a higher number of Au NPs per unit surface area. In the case of Au/μCeO_2, we anticipated that reducing the surface density of Au NPs could improve their stability because of (i) a more preferred nucleation and growth of the Au NPs on the relatively scarce defect sites of the μCeO_2 support during the deposition–precipitation process, and (ii) an increase in the interparticle spacing (*vide supra*). To validate our hypotheses, we synthesized a Au/μCeO_2 catalyst with a Au loading as low as 0.02 wt%. Since the dispersion for the 0.02 wt% Au/μCeO_2 (0.7) and that for the 0.5 wt% Au/μCeO_2 (0.6) were virtually identical, the former catalyst evidently had a significantly lower surface density of Au NPs. The performance of these catalysts and 0.4 wt% Au/$nCeO_2$ was investigated for a longer reaction time (72 h instead of 4–16 h) and a higher glucose/Au ratio (9000 instead of 140). Fig. 4 shows the turnover number (TON, defined as moles of glucose converted per mole of surface Au) as a function of reaction time. The results are in good agreement with the observation made in Fig. 1 that 0.4 wt% Au/$nCeO_2$ is found to be more stable than 0.5 wt% Au/μCeO_2. Although Au NPs supported on microsized metal oxides were initially as active as Au NPs supported on nanosized supports, their activity decreased due to sintering. Consistent with our previous findings, the increased maximum

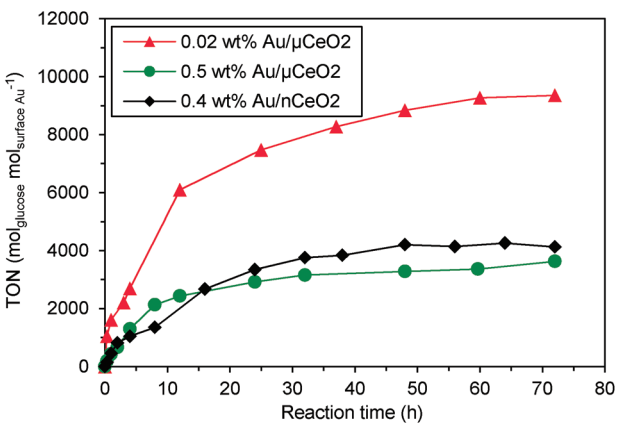

Fig. 4 Turnover number for glucose oxidation with 0.02 wt% Au/μCeO_2, 0.5 wt% Au/μCeO_2 and 0.4 wt% Au/$nCeO_2$ as a function of reaction time. Reaction conditions: glucose 167 mmol L^{-1}, 12 mL, pO_2 = 2.3 bar, 65 °C, glucose/Au = 9000.

TON of 9090 for 0.02 wt% Au/μCeO_2 shows that the lower surface density of the Au NPs indeed leads to a significantly higher activity and catalyst stability. A similar phenomenon was reported by Abad *et al.* while studying the influence of Au loading on the activity of Au/nCeO_2 for the base-free oxidation of cinnamyl alcohol in toluene.[34] They observed that the turnover frequency (TOF, defined as moles of substrate converted per mole of surface Au per hour) was more than three times higher for 0.44 wt% Au/nCeO_2 than for 1.80 wt% Au/nCeO_2, although both catalysts had almost the same particle size distribution.

3.4. Effect of the Au particle size on the turnover frequency

An important question concerning the impact of sintering is how the TOF relates to the mean diameter of the Au NPs.[45] Studies by Ishida *et al.* have previously demonstrated the size dependence of the TOF of Au supported on metal oxides for glucose oxidation at pH 9.[11] They inferred that the reaction might occur at the surface of the Au particles rather than at the interface between the Au NPs and the metal oxide support. Comparable trends were observed for the catalytic oxidation reactions performed under our reaction conditions (Fig. 5), which points to the more general nature of these findings. Au/nCeO_2, however, showed a significant decrease in TOF even for samples with almost the same mean diameter of Au NPs. This suggests that the deactivation may be caused by factors other than leaching or sintering of the Au NPs, such as the adsorption of reactive species on the Au surface.

3.5. Inhibition of the catalytic activity by adsorption of reactive species and regeneration by calcination

Compelling evidence for the adsorption of reactive species came from TGA and XPS analyses of the Au/μCeO_2 catalyst before and after reaction, as well as after calcination at 225 °C and 325 °C. The XPS spectra in Fig. 6 indicate that Au^0 is the predominant oxidation state of the Au NPs on the as-synthesized catalysts. The Au 4f signal shows two characteristic peaks at 87.5 eV and 83.8 eV, corresponding to Au $4f_{5/2}$ and Au $4f_{7/2}$ transitions, respectively. After reaction with glucose, both peaks shifted to lower binding energies compared to the as-synthesized sample. The negative shift (−0.5 eV) is tentatively attributed to the electron transfer from intermediate species to Au^0 on the surface of the Au NPs. This electronic perturbation can be anticipated from previous studies that showed a severe deactivation of Au NPs by the strong adsorption of ketone intermediates and condensation products of ketones.[46] The adsorption of species on the Au catalyst was also confirmed by TGA. Spent catalyst samples were washed with deionized water, dried at 80 °C and heated from room temperature to 600 °C under air while monitoring the weight losses (Fig. S2 in the ESI†). The decomposition occurred at temperatures up to 325 °C, which is why we chose to calcine the spent catalysts at this temperature. An additional calcination treatment was performed at 225 °C to diminish the possible effect of sintering.

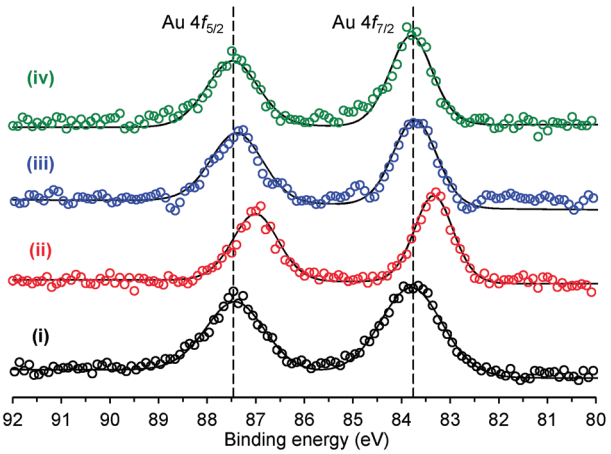

Fig. 6 XPS Au 4f spectra of (i) as-synthesized 0.02 wt% Au/μCeO_2, (ii) after 72 h of reaction with glucose and washing with deionized water, (iii) after regeneration by calcination at 225 °C and (iv) after regeneration by calcination at 325 °C. The open circles show raw experimental data. The C1s signal was shifted to 284.8 eV for charge correction.

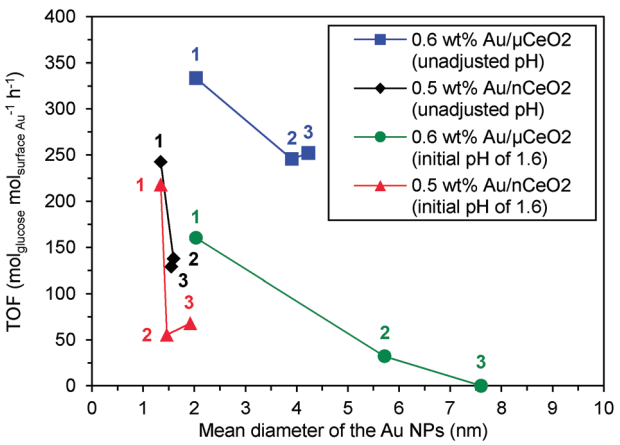

Fig. 5 TOF per surface Au atom as a function of the mean diameter of the Au NPs. The TOFs were measured after 20 min of reaction. Numbers 1–3 indicate data points corresponding to the as-synthesized catalyst, the catalyst recovered after the first cycle and the catalyst recovered after the last cycle in Fig. 1, respectively. Reaction conditions: see Fig. 1.

As shown in the XPS spectra (Fig. 6), the Au $4f_{5/2}$ and Au $4f_{7/2}$ peaks of the calcined samples gradually shifted back to the band energies of the as-synthesized catalyst. According to ICP-AES measurements, the recovered and regenerated catalysts ((ii), (iii) and (iv) in Fig. 6) had almost the same Au loading as the as-synthesized catalyst (i). Because of the similar electronic state and loading of Au for the as-synthesized catalyst and the one regenerated by calcination at 325 °C, it was expected that both catalysts would show a comparable catalytic activity. Our experiments, however, still showed a significant decrease in catalytic performance. Specifically, the initial TOF of the as-synthesized catalyst was 3100 $mol_{glucose}$ $mol_{surface\ Au}^{-1}$ h^{-1}, whereas the calcined sample showed an initial TOF of 760 $mol_{glucose}$ $mol_{surface\ Au}^{-1}$ h^{-1}. A reaction promoted by the calcined catalyst gave a conversion of 8% after 12 h, while the as-synthesized catalyst led to a

conversion of 43% under the same reaction conditions. Note that the catalyst calcined at 225 °C showed no significant catalytic activity.

Although part of the deactivation of Au/μCeO_2 can be ascribed to the inhibition by reactive species, the severe loss of activity after calcination at 325 °C is remarkable. Currently, we hypothesize that the most likely deactivation pathway is caused by agglomeration of the Au NPs, as the catalyst calcined at 325 °C (5.7 ± 5.5 nm) showed significantly larger particle sizes than the as-synthesized catalyst (1.7 ± 0.6 nm) (Fig. S3 in the ESI†). Consequently, larger particles may feature drastically lower amounts of the most active sites on the surface of the Au NPs. A future challenge to be addressed is to tailor the calcination conditions to remove the competitively adsorbed reactive species while preserving the original Au particle size distribution.

4. Conclusions

This work has shown that Au nanoparticles supported on metal oxides are active and selective catalysts for the oxidation of glucose to gluconic acid under base-free conditions. The stability study offers some clues to how the irreversible deactivation of the catalysts occurs through leaching and hydrothermal sintering of the Au nanoparticles. An easily applicable approach for improving the catalyst's stability against sintering is lowering the Au loading on the metal oxides. Our results indicate that the surface density of the Au nanoparticles affects their tendency to agglomerate during the oxidation reaction. Under the applied conditions, the highest stability was found for a 0.02 wt% Au/μCeO_2 catalyst prepared by the deposition–precipitation method. The reversible deactivation of this catalyst is ascribed to the adsorption of reactive species, which could be removed by calcination of the spent catalyst at 325 °C. Finally, our findings encourage further efforts to investigate the particle-size dependence of glucose oxidation under base-free conditions.

Acknowledgements

Y. W. and K. K. S. thank DuPont for financial support. S. V. d. V. thanks the Research Foundation – Flanders (FWO), the Belgian American Educational Foundation (BAEF), the "Plateforme pour l'Éducation et le Talent" and the Fulbright-Hays Commission for Educational Exchange between the United States and Belgium.

References

1 H. Hustede, H.-J. Haberstroh and E. Schinzig, in *Ullmann's Encyclopedia of Industrial Chemistry*, Wiley-VCH Verlag GmbH & Co. KGaA, 2000.
2 B. T. Kusema and D. Y. Murzin, *Catal. Sci. Technol.*, 2013, **3**, 297–307.
3 S. Van de Vyver and Y. Roman-Leshkov, *Catal. Sci. Technol.*, 2013, **3**, 1465–1479.
4 N. Thielecke, M. Aytemir and U. Prüsse, *Catal. Today*, 2007, **121**, 115–120.
5 N. M. Xavier, A. l. P. Rauter and Y. Queneau, *Top. Curr. Chem.*, 2010, **295**, 19–62.
6 C. Baatz and U. Prüße, *J. Catal.*, 2007, **249**, 34–40.
7 H. Kobayashi and A. Fukuoka, *Green Chem.*, 2013, **15**, 1740–1763.
8 C. D. Pina, E. Falletta and M. Rossi, *Chem. Soc. Rev.*, 2012, **41**, 350–369.
9 B. T. Kusema, B. C. Campo, P. Mäki-Arvela, T. Salmi and D. Y. Murzin, *Appl. Catal., A*, 2010, **386**, 101–108.
10 A. Mirescu and U. Pruesse, *Appl. Catal., B*, 2007, **70**, 644–652.
11 T. Ishida, N. Kinoshita, H. Okatsu, T. Akita, T. Takei and M. Haruta, *Angew. Chem., Int. Ed.*, 2008, **47**, 9265–9268.
12 S. Biella, L. Prati and M. Rossi, *J. Catal.*, 2002, **206**, 242–247.
13 N. Thielecke, K.-D. Vorlop and U. Prüße, *Catal. Today*, 2007, **122**, 266–269.
14 T. Ishida, K. Kuroda, N. Kinoshita, W. Minagawa and M. Haruta, *J. Colloid Interface Sci.*, 2008, **323**, 105–111.
15 V. Matveeva, A. Bykov, V. Doluda, M. Sulman, N. Kumar, S. Dzwigaj, E. Marceau, L. Kustov, O. Tkachenko and E. Sulman, *Top. Catal.*, 2009, **52**, 387–393.
16 Y. Önal, S. Schimpf and P. Claus, *J. Catal.*, 2004, **223**, 122–133.
17 C. Ma, W. Xue, J. Li, W. Xing and Z. Hao, *Green Chem.*, 2013, **15**, 1035–1041.
18 H. Yin, C. Zhou, C. Xu, P. Liu, X. Xu and Y. Ding, *J. Phys. Chem. C*, 2008, **112**, 9673–9678.
19 H. Okatsu, N. Kinoshita, T. Akita, T. Ishida and M. Haruta, *Appl. Catal., B*, 2009, **369**, 8–14.
20 I. V. Delidovich, B. L. Moroz, O. P. Taran, N. V. Gromov, P. A. Pyrjaev, I. P. Prosvirin, V. I. Bukhtiyarov and V. N. Parmon, *Chem. Eng. J.*, 2013, **223**, 921–931.
21 H. Zhang and N. Toshima, *Catal. Sci. Technol.*, 2013, **3**, 268–278.
22 X. Tan, W. Deng, M. Liu, Q. Zhang and Y. Wang, *Chem. Commun.*, 2009, 7179–7181.
23 D. An, A. Ye, W. Deng, Q. Zhang and Y. Wang, *Chem.–Eur. J.*, 2012, **18**, 2938–2947.
24 J. Zhang, X. Liu, M. N. Hedhili, Y. Zhu and Y. Han, *ChemCatChem*, 2011, **3**, 1294–1298.
25 S. Van de Vyver, J. Geboers, P. A. Jacobs and B. F. Sels, *ChemCatChem*, 2011, **3**, 82–94.
26 J. A. Geboers, S. Van de Vyver, R. Ooms, B. Op de Beeck, P. A. Jacobs and B. F. Sels, *Catal. Sci. Technol.*, 2011, **1**, 714–726.
27 M. Yabushita, H. Kobayashi and A. Fukuoka, *Appl. Catal., B*, DOI: 10.1016/j.apcatb.2013.01.052.
28 C. Baatz, N. Thielecke and U. Prüße, *Appl. Catal., B*, 2007, **70**, 653–660.
29 U. Prüße, M. Herrmann, C. Baatz and N. Decker, *Appl. Catal., A*, 2011, **406**, 89–93.

30 O. Casanova, S. Iborra and A. Corma, *J. Catal.*, 2009, **265**, 109–116.
31 M. Murdoch, G. I. N. Waterhouse, M. A. Nadeem, J. B. Metson, M. A. Keane, R. F. Howe, J. Llorca and H. Idriss, *Nat. Chem.*, 2011, **3**, 489–492.
32 A. Corma and H. Garcia, *Chem. Soc. Rev.*, 2008, **37**, 2096–2126.
33 M. Comotti, C. Della Pina, R. Matarrese and M. Rossi, *Angew. Chem., Int. Ed.*, 2004, **43**, 5812–5815.
34 A. Abad, A. Corma and H. Garcia, *Chem.–Eur. J.*, 2008, **14**, 212–222.
35 S. Van de Vyver, S. Helsen, J. Geboers, F. Yu, J. Thomas, M. Smet, W. Dehaen, Y. Román-Leshkov, I. Hermans and B. F. Sels, *ACS Catal.*, 2012, **2**, 2700–2704.
36 S. Van de Vyver, J. Geboers, S. Helsen, F. Yu, J. Thomas, M. Smet, W. Dehaen and B. F. Sels, *Chem. Commun.*, 2012, **48**, 3497–3499.
37 Y. Guan, D. A. J. M. Ligthart, Ö. Pirgon-Galin, J. A. Z. Pieterse, R. A. van Santen and E. J. M. Hensen, *Top. Catal.*, 2011, **54**, 424–438.
38 Q. Fu, A. Weber and M. Flytzani-Stephanopoulos, *Catal. Lett.*, 2001, **77**, 87–95.
39 Y. Lee, G. He, A. J. Akey, R. Si, M. Flytzani-Stephanopoulos and I. P. Herman, *J. Am. Chem. Soc.*, 2011, **133**, 12952–12955.
40 R. Si and M. Flytzani-Stephanopoulos, *Angew. Chem., Int. Ed.*, 2008, **47**, 2884–2887.
41 G. Prieto, J. D. Meeldijk, K. P. de Jong and P. E. de Jongh, *J. Catal.*, 2013, **303**, 31–40.
42 G. Prieto, J. Zecevic, H. Friedrich, K. P. de Jong and P. E. de Jongh, *Nat. Mater.*, 2013, **12**, 34–39.
43 L. K. Ono and B. Roldan-Cuenya, *Catal. Lett.*, 2007, **113**, 86–94.
44 N. Ta, J. Liu, S. Chenna, P. A. Crozier, Y. Li, A. Chen and W. Shen, *J. Am. Chem. Soc.*, 2012, **134**, 20585–20588.
45 A. Corma, P. Concepción, M. Boronat, M. J. Sabater, J. Navas, M. J. Yacaman, E. Larios, A. Posadas, M. A. López-Quintela, D. Buceta, E. Mendoza, G. Guilera and A. Mayoral, *Nat. Chem.*, 2013, **5**, 775–781.
46 B. N. Zope and R. J. Davis, *Green Chem.*, 2011, **13**, 3484–3491.

